This is a “preproof” accepted article for *Mineralogical Magazine*.

This version may be subject to change during the production process.

10.1180/mgm.2024.102

Steiningerite, $Ba_2Zr_2(Si_4O_{12})O_2$, a new cyclosilicate from the Löhley quarry, Germany

Rafał Juroszek[1]*, Biljana Krüger[2], Uwe Kolitsch[3,4], Günter Frenz[5], Günter Blaß[6]

[1]Institute of Earth Sciences, Faculty of Natural Sciences, University of Silesia, Będzińska 60, 41-205 Sosnowiec, Poland;

[2]Institute of Mineralogy and Petrography, University of Innsbruck, Innrain 52, 6020 Innsbruck, Austria;

[3]Mineralogisch-Petrographische Abteilung, Naturhistorisches Museum Wien, Burgring 7, A-1010, Wien, Austria;

[4]Institut für Mineralogie und Kristallographie, Universität Wien, Josef-Holaubek-Platz 2, A-1090 Wien, Austria;

[5]Private Collector, Börschgasse 16a, D-51143 Köln, Germany;

[6]Private Collector, Merzbachstr. 6, D-52249 Eschweiler, Germany;

* Author for correspondence: Rafał Juroszek, Email: rafal.juroszek@us.edu.pl

Abstract:

The new mineral steiningerite, ideally $Ba_2Zr_2(Si_4O_{12})O_2$, was discovered along fissures and in cavities in melilite nephelinite samples retrieved from the currently active Löhley quarry, Eifel Volcanic Fields, Germany. Steiningerite is associated with minerals of the pyroxene group (augite-diopside), leucite, perovskite, titanite and accessory fluorapatite, fresnoite, wöhlerite, götzenite, fersmanite, magnetite and minerals of the pyrochlore group. It usually forms colourless or creamy white, euhedral, short prismatic to thick tabular, partly pseudocubic crystals up to 100 μm in size but also rarely occurs as individuals reaching 0.5 mm in size. The mineral is transparent to translucent, exhibits vitreous lustre and no visible cleavage. The calculated density of steiningerite is 3.78 g/cm^3. Optically, steiningerite is non-pleochroic and uniaxial positive, with $\omega = 1.711(3)$, $\varepsilon = 1.750(3)$ ($\lambda = 589$ nm). The empirical formula of holotype steiningerite, calculated on 14 anions, is $(Ba_{1.36}K_{0.56}Na_{0.09}Sr_{0.05}Ca_{0.02})_{\Sigma 2.08}(Zr_{1.52}Ti_{0.25}Nb_{0.13}U_{0.05}Fe_{0.02}Hf_{0.01})_{\Sigma 1.98}(Si_{4.00}Al_{0.03})_{\Sigma 4.03}O_{12}(O_{1.59}F_{0.41})_{\Sigma 2.00}$. Steiningerite crystallises in space group *P4/mbm*, with refined unit-cell parameters $a = 8.894(2)$ Å, $c = 8.051(2)$ Å, $V = 636.9(3)$ Å^3, $Z = 2$. The crystal structure, determined from single-crystal intensity data, was refined to $R = 0.0310$ for 444 unique reflections with $I > 3\sigma(I)$. The mineral is isotypic with the synthetic $KTaSi_2O_7$ and structurally similar to the mineral rippite, $K_2(Nb,Ti)_2(Si_4O_{12})(O,F)_2$. The hetero-polyhedral framework is formed by the chains of $(Zr,Ti)O_6$ octahedra, running parallel to the four-fold axis, which are combined via Si_4O_{12} rings. Each $(Zr,Ti)O_6$ octahedron shares four vertices with four SiO_4 tetrahedra, belonging to four different Si_4O_{12} units. This arrangement of atoms creates channels along the *c* axis, with a pentagonal cross-section, in which charge-balancing Ba^{2+} and K^+ ions are located. Extra-framework alkaline and alkaline-earth cations have twelve-fold coordination. The occurrence of the new mineral in a melilite nephelinite, along with its high-temperature

https://doi.org/10.1180/mgm.2024.102 Published online by Cambridge University Press

mineral association and the absence of H_2O and OH groups, confirmed by Raman and FTIR spectroscopies, indicate high-temperature conditions of formation and suggests a pneumatolytic origin of steiningerite.

Keywords: Steiningerite, new mineral species, cyclosilicate, crystal structure, Löhley quarry, Eifel, Germany

Introduction

Steiningerite, ideally $Ba_2Zr_2(Si_4O_{12})O_2$, a new cyclosilicate mineral, was discovered within fissures and cavities of melilite nephelinite samples in the currently active Löhley quarry (50°9'33" N, 6°48'41" E), Üdersdorf, near Daun, in the Eifel Volcanic Fields of Rhineland-Palatinate, Germany. The steiningerite-bearing rock samples were collected in 1990 by Günter Blaβ, Jochen Tschörtner and other collectors, and were preliminarily investigated with chemical-analytical data, optical measurements and a crystal-structure determination (R = 1.5%, crystal size 0.12 x 0.12 x 0.13 mm), by Kolitsch et al. (2003), based on a few crystals collected by Franz-Josef Emmerich. Additional sample collection was done in 2021 by Günter Frenz, and his specimen is the holotype for steiningerite. Steiningerite is isotypic with the synthetic compound $KTaSi_2O_7$ (Lee et al. 1996) and closely related to the ferroelectric compound $KNbSi_2O_7$ (space group *P*4*bm*, Crosnier et al. 1991, 1992; Foster et al. 1999), which is a synthetic analogue of the recently described mineral rippite, $K_2(Nb,Ti)_2(Si_4O_{12})(O,F)_2$ (Sharygin et al. 2020). Kolitsch et al. (2003) briefly pointed out a structural relation of these phases to the members of the nenadkevichite group (pseudo-tetragonal).

The name steiningerite is given in honour of Johannes (Johann) Steininger (born 10

https://doi.org/10.1180/mgm.2024.102 Published online by Cambridge University Press

January 1794 in St. Wendel, died 11 October 1874 in Trier), a German professor, geologist and historian who was a pioneer of Luxembourg geology. Steininger was a person with multiple interests; in addition to geology, he also dealt with other natural sciences as well as history and philosophy. His field work in Eifel (Germany), Belgium, France and Luxembourg led to significant discoveries. Notably, in 1853, he described a fossil *Spirifera primaeva*, a brachiopod species now known as *Acrospirifer primaevus*. Moreover, during a research expedition to the Saar-Nahe area in 1841, he described as "Tholeiit" the "doleritic trappstone" of Schaumberg mountain near Tholey/Saar. This name was subsequently used as the petrographic term for the most common rock of the Earth's crust, the basalt of the Mid-Ocean Ridge ("MOR basalt" or MORB).

The new mineral (IMA2024-016), its name and symbol (Sngr) were subsequently approved by the Commission on New Minerals, Nomenclature and Classification (CNMNC) of the International Mineralogical Association (IMA).

The present paper provides a detailed characterisation of steiningerite from the Löhley quarry, including chemical, structural and spectroscopic data, as well as a discussion of structurally related phases and the condition of formation of the new mineral species. The holotype material with steiningerite is deposited in the Natural History Museum Mainz, State Collection for Natural History Rhineland-Palatinate, Reichklarstrasse 10, D-55116 Mainz, Germany, with the catalogue number NHMMZ M 2024/1-LS.

Methods of investigation

The chemical composition, crystal morphology and optical properties of steiningerite and associated minerals were studied using an optical microscope and a Phenom XL analytical scanning electron microscope (SEM; Institute of Earth Sciences, Faculty of Natural Sciences, University of Silesia, Sosnowiec, Poland). In turn, quantitative electron probe microanalyses

https://doi.org/10.1180/mgm.2024.102 Published online by Cambridge University Press

(EPMA) were carried out on CAMECA SX100 (Micro-Area Analysis Laboratory, Polish Geological Institute, National Research Institute, Warsaw, Poland) at 15 kV and 40 nA, with a beam diameter of ~1 μm, using the following lines and standards: Nb*L*α – Nb; Si*K*α, Ca*K*α – wollastonite; Ti*K*α – titanite; Zr*L*α, Hf*L*α – zircon; U*M*α – U-glass-3; Sr*L*α – $SrTiO_3$; K*K*α, Al*K*α – orthoclase; Fe*K*α – hematite; Ba*L*β – baryte; Na*K*α – NaCl; F*K*α – apatite.

The Raman spectrum of steiningerite was recorded on a WITec alpha 300R Confocal Raman Microscope (Institute of Earth Sciences, Faculty of Natural Sciences, University of Silesia, Sosnowiec, Poland) equipped with an air-cooled 488 nm solid-state laser and a CCD camera operating at -61˚C. The laser radiation was coupled to the microscope via a single-mode optical fibre with a diameter of 3.5 μm. A Zeiss air objective (L.D. EC Epiplan-Neofluan DIC-100/0.75NA) was used. The Raman scattered light was focused by an effective pinhole diameter of approximately 30 μm and a monochromator with a 600 mm^{-1} grating. The laser power at the sample position was 42 mW. The signal was recorded between 75 and 4000 cm^{-1} in a 180° backscatter geometry. Integration times of 10 s with an accumulation of 15 scans were chosen, and the resolution was 3 cm^{-1}. The spectrum was processed using the Spectracalc software package GRAMS (Galactic Industries Corporation, NH, USA). The Raman bands were fitted using a Gauss-Lorentz cross-product function with the minimum number of component bands used for the fitting process.

Infrared reflectance spectra were acquired from *in situ* crystals using a Nicolet iN10 infrared microscope (ThermoScientific) equipped with an LN-cooled MCT detector cooled to 77 K. Spectra were collected over the range of 4000–500 cm^{-1} with a resolution of 4 cm^{-1} using a 15x objective. A gold-covered reference slide spectrum was used as a background, and the sample spectrum was recorded by averaging 128 scans. Reflectance data were then converted to standard absorption spectra using Kramers-Krönig transformations.

Single-crystal X-ray studies of steiningerite were carried out on a two-circle IPDS II Stoe

https://doi.org/10.1180/mgm.2024.102 Published online by Cambridge University Press

diffractometer equipped with an Imaging Plate detector (Institute of Mineralogy and Petrography, University of Innsbruck, Austria). The measurement was performed at ambient conditions (293 K), and the data were collected using Mo*K*α radiation (λ = 0.71073 Å). The determination of unit-cell parameters and data reduction were performed using X-Area software (STOE & Cie GmbH 2018). The structure solution and refinement were performed using Superflip (Palatinus and Chapuis, 2007) and Jana2020 programs (Petříček et al. 2023). Further details concerning data collection and refinement are given in Table 1. The atom coordinates, site occupancies, displacement parameters and main bond lengths are listed in Tables 3-5 in the Crystal structure section as well as in the CIF (Crystallography Information File) reported in Supplementary Materials.

Table 1. Crystal data, data collection information and refinement details for steiningerite.

Crystal Data	
Refined structural formula	$(Ba_{1.29}K_{0.71})(Zr_{1.89}Ti_{0.11})(Si_4O_{12})O_2$
Space group	*P*4/*mbm*
Unit-cell parameters (Å)	*a* = 8.894(2)
	c = 8.051(2)
Volume (Å^3)	*V* = 636.9(3)
Z	2
D_{calc} (g/cm^3)	3.78
μ (mm^{-1})	6.207
F_{000}	664
Crystal size (μm)	50 × 40 × 30
Data collection	
Diffractometer	IPDS Stoe
Radiation type	Mo*K*α
λ (Å)	0.71073
Detector	Imaging Plate
Temperature (K)	293
θ range (˚)	3.24-29.18
Index ranges	$-12 \le h \le 10$
	$-7 \le k \le 12$
	$-11 \le l \le 9$
No. of measured reflections	2098
No. of unique reflections	502
Refinement of the structure	
No. of obs. unique refl. [$I > 3\sigma(I)$]	444

https://doi.org/10.1180/mgm.2024.102 Published online by Cambridge University Press

No. of parameters	37
R_{int}	0.0292
R_1 (obs.) / R_1 (all)	0.0310 / 0.0397
*wR_2 (obs.) / wR_2 (all)	0.0841 / 0.0917
GOF (obs.) / GOF (all)	2.91 / 2.85
$\Delta\rho_{max}$ / $\Delta\rho_{min}$ (e Å^{-3})	1.34 / -1.12

*wR_2 (Weighting scheme) : $w = 1/(\sigma^2(F) + 0.0001F^2)$

Occurrence, mineral association, physical and optical properties of steiningerite

The rock samples containing steiningerite were collected in the operating Löhley quarry (50°9'33" N, 6°48'41" E), near the settlement of Üdersdorf, near Daun, Eifel Volcanic Fields, Rhineland-Palatinate, Germany (Fig. 1a). The studied volcanic rocks from this locality belong to one of the numerous volcanoes active in the Pleistocene (Lengauer et al. 2001). In contrast to the xenolith-rich lava of the Bellerberg volcanic area, mineral assemblages from Löhley are found in cavities, fissures and pegmatite-like veins within the host melilite nephelinite (Fig. 1b; Mertes 1983; Hentschel, 1987). The Löhley quarry is the type locality for four other mineral species: batiferrite, $BaTi_2Fe^{3+}{}_8Fe^{2+}{}_2O_{19}$ (Lengauer et al. 2001); noonkanbahite, $NaKBaTi_2(Si_4O_{12})O_2$ (Uvarova et al. 2010); schüllerite, $Ba_2Ti_2Na_2Mg_2(Si_2O_7)_2O_2F_2$ (Chukanov et al. 2011), and lileyite, $Ba_2Ti_2Na_2Fe^{2+}Mg(Si_2O_7)_2O_2F_2$ (Chukanov et al. 2012).

Fig. 1. a) View of the steiningerite holotype location – the Löhley quarry, Üdersdorf, Eifel Volcanic Fields, Germany, (photo: Frank de Wit); b) Fragment of the holotype rock specimen

https://doi.org/10.1180/mgm.2024.102 Published online by Cambridge University Press

containing steiningerite.

Steiningerite from the Löhley quarry occurs in fissures filled mostly by colourless isometric leucite crystals, dark green tabular clinopyroxene and black isometric perovskite whose sizes are all a few mm (Fig. 1b). Minerals of the pyroxene group are mainly represented by augite and diopside. Locally, brown elongated crystals of titanite and yellow tabular crystals of fresnoite, $Ba_2TiO(Si_2O_7)$ also are present. Fluorapatite, wöhlerite, götzenite, fersmanite, magnetite and minerals of the pyrochlore group, primarily fluorcalciopyrochlore, are noted as accessory phases.

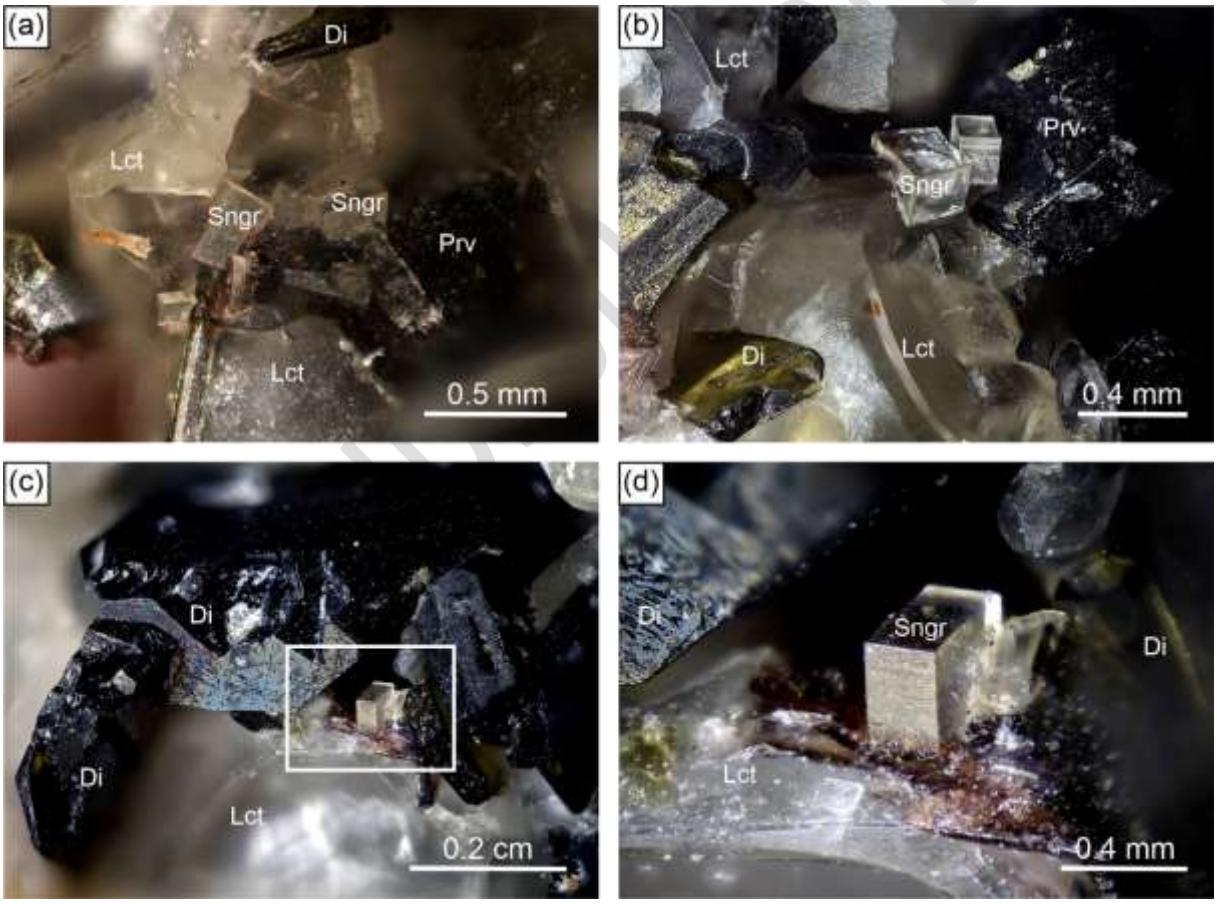

Fig. 2. (a-d) Microphotographs of transparent crystals of steiningerite and associated minerals in the holotype specimen; framed section in (c) is magnified in (d); photos: Volker Heck. Mineral abbreviations: Di – diopside; Lct – leucite; Prv – perovskite; Sngr – steiningerite.

https://doi.org/10.1180/mgm.2024.102 Published online by Cambridge University Press

Steiningerite crystals typically exhibit a euhedral, short prismatic to thick tabular, partly pseudocubic habit. The maximum size of individual crystals in the holotype specimen reaches 0.5 mm (Fig. 2a-d), although crystals of this size are relatively rare. In general, steiningerite crystals are smaller, and their size does not exceed 100 μm (Fig. 3a-d). In most cases, steiningerite crystallised on isometric perovskite crystals (possibly as epitactic overgrowth) or in immediate contact with them (Fig. 3a-c). Occasionally, the new mineral is also observed on leucite crystals (Fig. 3d).

Steiningerite is transparent to translucent, creamy white or colourless, with a vitreous lustre and white streak (Fig. 2). It is brittle with an uneven fracture observed under the scanning electron microscope (Fig. 3). Cleavage or parting were not observed. The mineral exhibits a weak orange fluorescence under ultraviolet light (λ = 254 nm). Micro-hardness indentation of steiningerite crystals was carried out using a load of 10 g, which gave a mean value for the VHN (Vickers Hardness Number) of 305.3 kg/mm^3 (range from 262 to 332 kg/mm^3, based on 15 measurements). A hardness of 3.5-4 on the Mohs scale corresponds to the obtained result.

The calculated density based on the empirical formula and single-crystal unit-cell parameters is 3.78 g/cm^3. A previous, unpublished measurement of density on the crystal studied by Kolitsch et al. (2003) gave a value of 3.68(3) g/cm^3, close to the crystal's X-ray density of 3.711 g/cm^3 and the density calculated from subsequently measured EPMA data, 3.65 g/cm^3. This difference between samples is caused by the variations in chemical composition (see below for details). Optically, steiningerite is non-pleochroic and uniaxial positive with ω = 1.711(3), ε = 1.750(3) (λ = 589 nm). For the crystal studied by Kolitsch et al. (2003), the values are slightly different, with ω = 1.681(2) and ε = 1.771(5). For the calculated formula, the Gladstone-Dale compatibility index (Mandarino, 1989) of holotype steiningerite is 1 – (Kp/Kc) = -0.014 (superior).

https://doi.org/10.1180/mgm.2024.102 Published online by Cambridge University Press

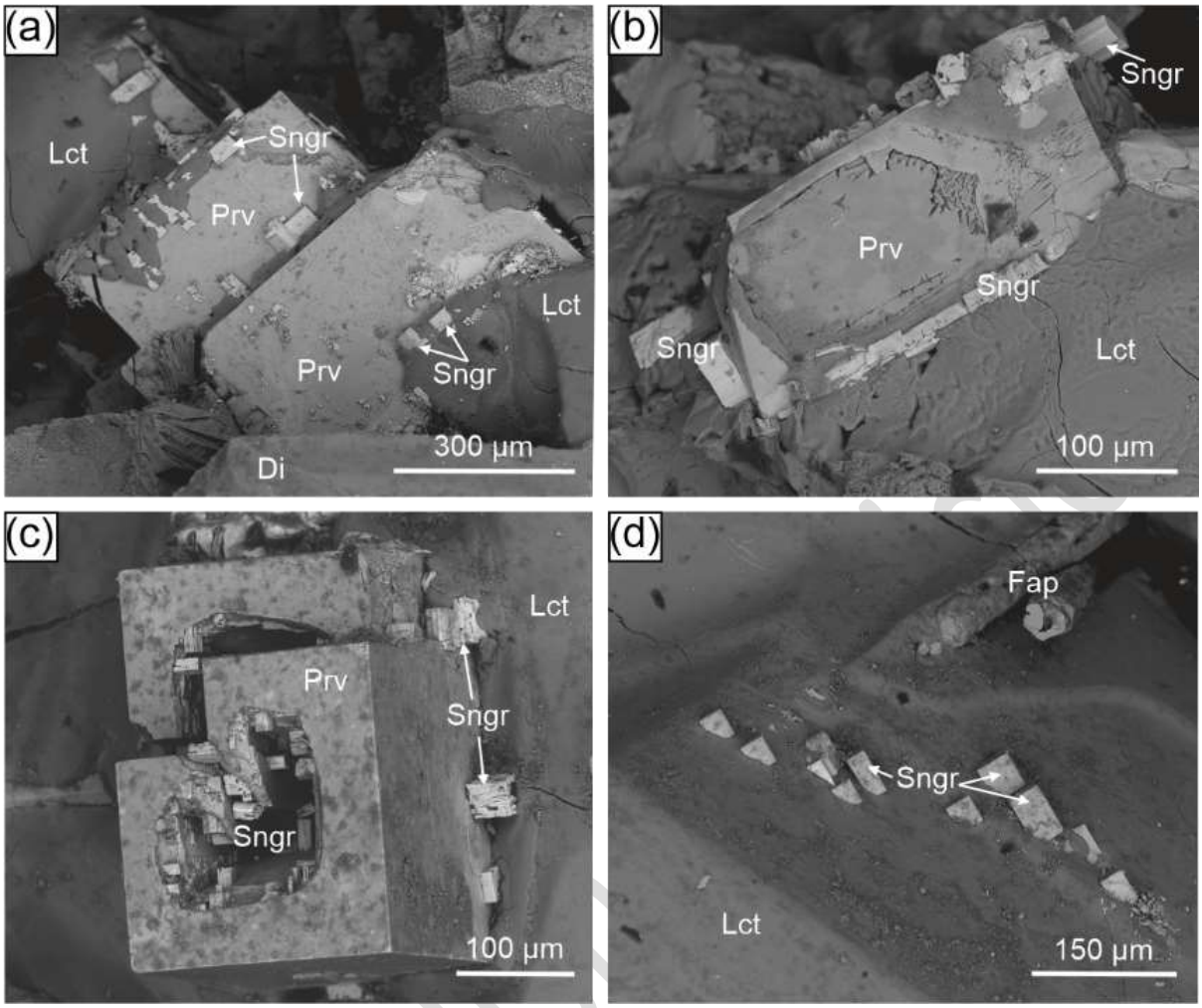

Fig. 3. BSE (back-scattered electron) images of euhedral steiningerite crystals crystallising on perovskite (a-c) and leucite crystals (d). Mineral abbreviations: Di – diopside; Fap – fluorapatite; Lct – leucite; Prv – perovskite; Sngr – steiningerite.

Results

Chemical composition

The results of the electron microprobe analyses of holotype steiningerite are presented in Table 2. The empirical formula calculated based on 14 anions is $(Ba_{1.36}K_{0.56}Na_{0.09}Sr_{0.05}Ca_{0.02})_{\Sigma 2.08}(Zr_{1.52}Ti_{0.24}Nb_{0.13}U_{0.05}Al_{0.03}Fe_{0.02})_{\Sigma 1.98}Si_{4.00}O_{12}(O_{1.59}F_{0.41})_{\Sigma 2.00}$,

https://doi.org/10.1180/mgm.2024.102 Published online by Cambridge University Press

which leads to the following simplified formula: $(Ba,K,Na,Sr,Ca)_2(Zr,Ti,Nb,U,Fe,Al)_2Si_4O_{12}(O,F)_2$. The ideal end-member formula $Ba_2Zr_2(Si_4O_{12})O_2$ corresponds to 38.65 wt% of BaO, 31.06 wt% of ZrO_2, and 30.29 wt% of SiO_2. The ideal formula could also be simplified to $BaZrSi_2O_7$, but this would obscure the fact that the mineral is a cyclosilicate. Previous EPMA data for the same material from the Löhley quarry (Table 2) gave the chemical formula $(Ba_{1.37}K_{0.52}Na_{0.09}Ca_{0.02})_{\Sigma 2.00}(Zr_{1.43}Ti_{0.40}Al_{0.06})_{\Sigma 1.89}Si_{4.14}O_{12}(O_{1.39}F_{0.61})_{\Sigma 2.00}$, which is fairly close to the holotype, but with a slightly lower Zr:Ti ratio, and an anomalously high Si content (checked but not detected were: Mg, Sr, B, V, Nb, Ta, Y, Sc, La, Ce). The total was only 94.6 wt% for unknown reasons (the presence of either OH or H_2O, or both, was tentatively assumed, but could not be corroborated by subsequent Raman spectroscopic studies, unfortunately hampered by fluorescence), and a slight chemical zonation was noted (Kolitsch et al. 2003). Chemical data of the investigated steiningerite crystals obtained by EPMA show significant substitution on the Ba^{2+} polyhedral site on which Ba^{2+} is substituted by monovalent cations, mainly K^+ (Table 2). Such substitution generates charge instability that must be balanced by the presence of F^-, which can replace O^{2-} partially. More probable is the isomorphic substitution scheme $Ba^{2+} + Zr^{4+} \leftrightarrow K^+ + Nb^{5+}$, which is indeed observed in steiningerite. This scheme is related to the steiningerite-rippite series. The highest measured amount of Nb_2O_5 is 4.76 wt%, corresponding to 0.26 Nb^{5+} pfu in the octahedrally coordinated site (spot 7, Table 2). Some of the analyses obtained from steiningerite indicate a locally increased amount of TiO_2 and UO_2 (spots 7 and 1 in Table 2). The highest amount of TiO_2 equals 4.30 wt%, and for UO_2, it is 3.77 wt%, corresponding to 0.40 Ti^{4+} pfu and 0.10 U^{4+}pfu, respectively. The presence of additional tetravalent elements and Nb_2O_5 are in line with a deficiency of ZrO_2 in analysed crystals, confirming that these elements substitute Zr^{4+} on the octahedrally coordinated site. The highest observed amount of ZrO_2 (spot 6, Table 2) equals

https://doi.org/10.1180/mgm.2024.102 Published online by Cambridge University Press

29.20 wt% and corresponds to 1.75 Zr^{4+} pfu in the empirical formula. In addition, the EPMA data clearly suggest the incorporation of Nb and F in the structure of steiningerite via the heterovalent substitution scheme $Zr^{4+} + F^{+} \leftrightarrow Nb^{5+} + O^{2-}$. Moreover, the observed substitution of K^{+} for Ba^{2+}, Ti^{4+}/U^{4+} for Zr^{4+} and F^{-} for O^{2-} in steiningerite indicates the possibility of the theoretical end-members $K_2Zr_2(Si_4O_{12})F_2$, $K_2Ti_2(Si_4O_{12})F_2$ and $K_2U_2(Si_4O_{12})F_2$ which would entail the presence of a $(Zr,Ti,U)O_4F_2$ octahedron.

Table 2. Chemical analytical data (in wt%) for steiningerite.

Constituent	Mean (n = 16)	S.D.	Range	Spot 7♠	Spot 6♦	Spot 1♣	Mean* (n = 4)
Nb_2O_5	2.36	1.43	0.96-4.76	4.76	0.96	4.56	n.d.
SiO_2	32.48	0.22	32.25-33.12	32.25	32.59	32.25	33.19
TiO_2	2.65	0.89	1.68-4.30	4.30	1.68	3.59	4.24
ZrO_2	25.42	3.35	20.08-29.20	20.08	29.20	20.69	23.45
HfO_2	0.14	0.06	0.07-0.27	0.10	0.20	0.07	n.d.
UO_2	1.78	1.08	0.47-3.77	3.11	0.47	3.77	n.d.
Al_2O_3	0.20	0.04	0.13-0.29	0.29	0.17	0.22	0.38
Fe_2O_3	0.22	0.11	0.09-0.40	0.40	0.09	0.31	n.d.
CaO	0.15	0.06	0.09-0.25	0.24	0.11	0.20	0.15
BaO	28.17	0.36	27.55-28.77	27.56	28.07	27.55	28.02
SrO	0.69	0.28	0.40-1.19	1.19	0.51	0.95	n.d.
Na_2O	0.38	0.08	0.30-0.51	0.51	0.30	0.49	0.38
K_2O	3.59	0.14	3.31-3.77	3.31	3.71	3.50	3.27
F	1.06	0.10	0.93-1.29	0.96	1.01	1.04	1.56
Total	99.29			99.06	99.07	99.19	94.63
O = -F	0.45			0.40	0.43	0.44	0.65
Total	98.84			98.66	98.64	98.75	93.98
Calculated on 14 anions per formula unit							
Ca^{2+}	0.02			0.03	0.01	0.03	0.02
Ba^{2+}	1.36			1.32	1.35	1.33	1.37
Sr^{2+}	0.05			0.08	0.04	0.07	
Na^{+}	0.09			0.12	0.58	0.12	0.09
K^{+}	0.56			0.52	0.07	0.55	0.52
Sum A	**2.08**			**2.07**	**2.05**	2.10	**2.00**
Nb^{5+}	0.13			0.26	0.05	0.25	
Ti^{4+}	0.24			0.40	0.16	0.33	0.40
Zr^{4+}	1.52			1.20	1.75	1.24	1.43
Hf^{4+}	<0.01			<0.01	0.01	<0.01	
U^{4+}	0.05			0.08	0.01	0.10	
Al^{3+}	0.03			0.04	0.02	0.03	0.06
Fe^{3+}	0.02			0.04	0.01	0.03	

https://doi.org/10.1180/mgm.2024.102 Published online by Cambridge University Press

Sum B	**1.99**	**2.02**	**2.01**	**1.98**	**1.89**
Sum T (Si^{4+})	**4.00**	**3.96**	**4.01**	**3.98**	**4.14**
F^-	0.41	0.37	0.39	0.41	0.61
O^{2-}	1.59	1.63	1.61	1.59	1.39
Sum X	**2.00**	**2.00**	**2.00**	**2.00**	**2.00**

Notes: S.D. = 1σ = standard deviation; n = number of analyses; n.d. – not detected; ♠ analysis with the highest concentration of Nb_2O_5 and TiO_2; ♦ analysis with the highest concentration of ZrO_2; ♣ analysis with the highest concentration of UO_2; * Kolitsch et al. (2003)

Raman and FTIR spectroscopy data

In the Raman spectrum of steiningerite (Fig. 4), the spectral region ~850-1200 cm^{-1} is related to symmetric and asymmetric vibrations of the Si_4O_{12} building unit. More specifically, the strongest band at 956 cm^{-1} with a shoulder at 924 cm^{-1} is assigned to the internal symmetric stretching vibrations of SiO_3 (non-bridging oxygen atoms of SiO_4 tetrahedra). Two components between 1036 and 1064 cm^{-1} and a band at 1116 cm^{-1} are attributed to the asymmetric stretching Si–O–Si vibrations (bridging oxygen between two Si-centred tetrahedra). In turn, bands between 736 cm^{-1} and 846 cm^{-1} are related to the asymmetric stretching modes of SiO_3. The bridging symmetric stretching Si–O–Si vibrations correspond to the Raman bands in the 623-669 cm^{-1} spectral region. Several Raman bands with variable intensities at 419, 432 and 473 cm^{-1} are assigned to the asymmetric bending modes of SiO_3 and the in-plane bending vibrations of internal Si–O–Si, which are coupled with the Ba^{2+} translations. In general, bands below 360 cm^{-1} are related to deformation vibrations in $(Ba,K)O_{12}$ polyhedra and $(Zr,Ti)O_6$ octahedra as well as librational vibrations of Si_4O_{12} rings. Lattice vibrations are recorded below 150 cm^{-1} in the spectrum of steiningerite.

https://doi.org/10.1180/mgm.2024.102 Published online by Cambridge University Press

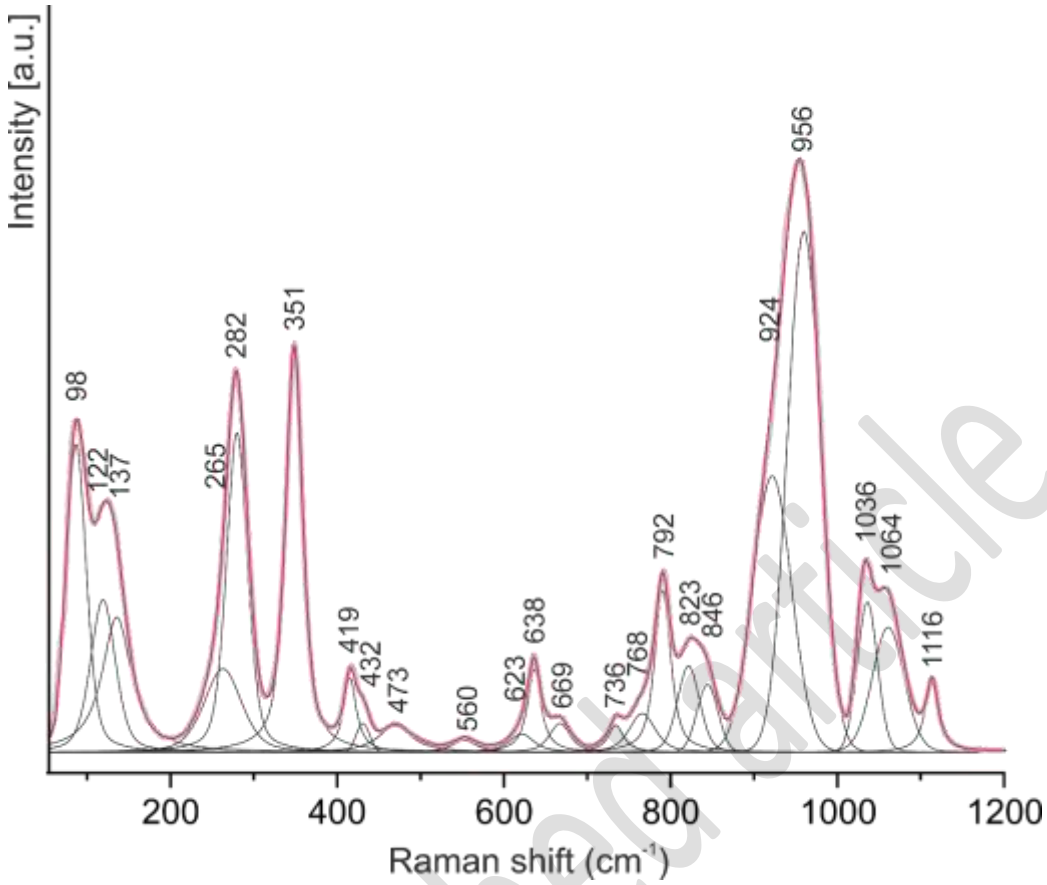

Fig. 4. Raman spectrum of steiningerite.

The FTIR spectrum of steiningerite (Fig. 5) is dominated by the strongest absorption band at 1003 cm^{-1}, which is assigned to the ν_3 internal stretching vibrations of the SiO_4 tetrahedra. The stretching vibrations of Si-O bonds in SiO_3 (non-bridging oxygen atoms of SiO_4 tetrahedra) and asymmetric stretching vibrations of Si-O-Si (bridging oxygen between two Si-centred tetrahedra) are active between 1003-1213 cm^{-1}. In the case of asymmetric stretching vibrations, the higher wavenumbers correspond to the vibrations of Si-O-Si involving a fragment with the Si-O-Si angle close to 180˚, whereas lower wavenumbers are related to smaller Si-O-Si angles (Chukanov 2014). Therefore, the band at 1213 cm^{-1} corresponds to asymmetric stretching vibrations of the fragment Si1-O5-Si1, in which the Si-O-Si angle equals 180˚ in the steiningerite structure (CIF). The absorption band at 663 and the weak band at 789 cm^{-1} are attributed to the symmetric stretching modes of the Si-O-Si bonds. The

https://doi.org/10.1180/mgm.2024.102 Published online by Cambridge University Press

stretching vibrations of Zr-O bonds in the ZrO_6 octahedra occur between 615-665 cm^{-1} in the spectral region. The band at 663 cm^{-1}, also related to the ZrO_6 octahedra, thus may overlap the symmetric stretching vibrations of the Si-O-Si linkage. The bands below 600 cm^{-1} in the IR spectrum are related to the Si-O bending vibrations and stretching modes arising from the Ba-O vibrations. There is no evidence of an absorption band between the 3000-4000 cm^{-1} region, thus excluding the presence of H_2O or OH groups in the structure.

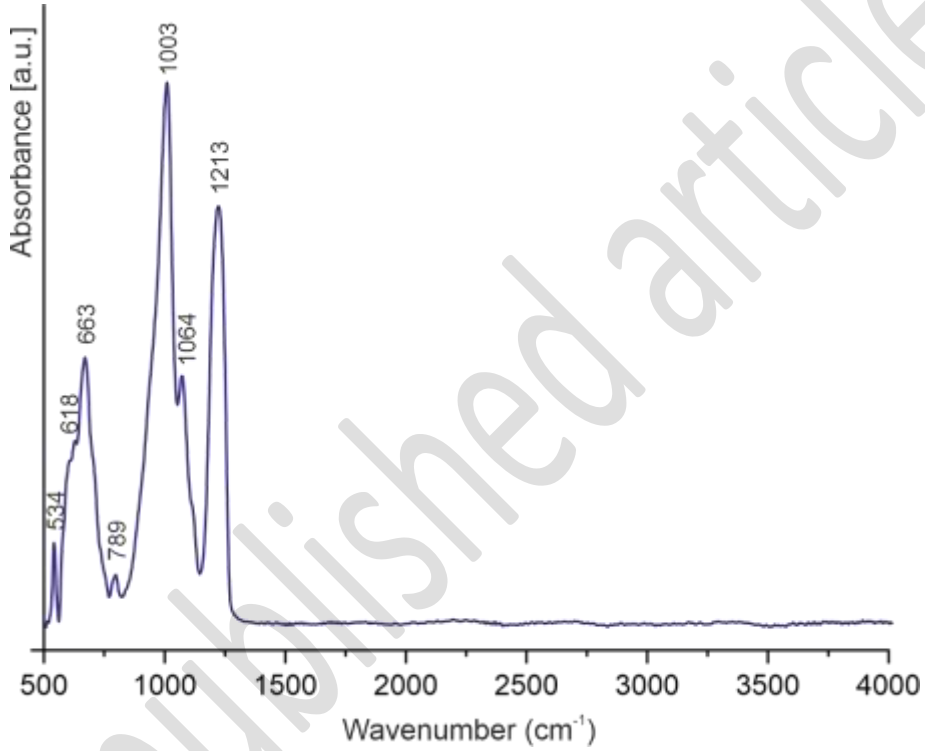

Fig. 5. FTIR spectrum of steiningerite crystal.

Crystal structure of steinigerite

Steiningerite is a cyclosilicate. The crystal structure of the new mineral has been solved using the charge-flipping method and refined to R = 0.0310 in the space group $P4/mbm$ with the unit-cell parameters a = 8.894(2) Å, c = 8.051(2) Å, V = 636.9(3) $Å^3$, Z = 2. Results of the previous refinement (a = 8.901(1) Å, c = 8.074(1) Å and V = 639.7(1) $Å^3$, Z = 4; Kolitsch et al. 2003) are in good agreement with the obtained data.

https://doi.org/10.1180/mgm.2024.102 Published online by Cambridge University Press

The asymmetric unit contains one Ba, one Zr, one Si and five O sites. All are located at special positions except O4. The three-dimensional framework of steiningerite consists of $(Ba,K)O_{12}$ polyhedra, $(Zr,Ti)O_6$ octahedra and SiO_4 tetrahedra linked into four-membered Si_4O_{12} rings approximately parallel to [110] (Fig. 6a). The $(Zr,Ti)O_6$ octahedra share vertices to form infinite chains parallel to the axes of four-fold symmetry; they are then vertex-connected to the SiO_4 tetrahedra forming the Si_4O_{12} rings (Fig. 6a). Each $(Zr,Ti)O_6$ octahedron shares four vertices with four SiO_4 tetrahedra, each belonging to four different Si_4O_{12} units, resulting in the three-dimensional framework (Fig. 6a). This structural arrangement creates channels with a pentagonal cross-section along the c axis, in which charge-balancing Ba^{2+} and K^+ ions are located (Fig. 6b).

The Ba^{2+} cations are partially replaced by K^+ cations, with a refined site-occupancy of $Ba_{0.645(8)}K_{0.355(8)}$ (Table 3), which are in good agreement with the empirical formula. These large cations are coordinated by twelve O atoms in an arrangement resembling two-capped pentagonal prisms. The interatomic (Ba,K)–O bond lengths range from 2.836(4) Å to 3.259(1) Å, with an average of 2.996 Å (Table 5). A partial substitution of Ti^{4+} for Zr^{4+} is also observed at the octahedrally coordinated site. The occupancy refinement of this site converged to a Zr:Ti ratio of 0.944(16):0.056(16) (Table 3), again in good agreement with the empirical formula. The Zr^{4+} and Ti^{4+} cations are coordinated by four O4 atoms in the equatorial plane with a (Zr,Ti) –O bond length equal to 2.074(3) Å, and two apical anions, O1 [at 2.0677(13) Å] and O2 [at 1.9577(13) Å]. The average (Zr,Ti)–O bond length is 2.053 Å (Table 5). Owing to the cation substitution, the average bond is shorter than ideal Zr–O bonds and longer than ideal Ti–O bonds. The SiO_4 tetrahedra in the Si_4O_{12} rings are connected via the ligands O3 and O5, whereas each O4 ligand, located at the eight outward-pointing vertices of the ring of tetrahedra, vertex-links with the $(Zr,Ti)O_6$ octahedra. The SiO_4 tetrahedron is quite regular and the Si–O bond length ranges from 1.5952(18) Å to 1.641(3) Å, with a Si–O

https://doi.org/10.1180/mgm.2024.102 Published online by Cambridge University Press

mean bond length of 1.608 Å (Table 5).

The cation site-populations of the empirical formula (normalized to 1.00) were used to calculate the weighted bond valences (Table 5) utilizing the program ECoN21 (Ilinca 2022). The (Ba1,K1) site, with empirical occupancy ($Ba_{0.65}K_{0.28}Na_{0.04}Sr_{0.02}Ca_{0.01}$) and weighted formal charge of 1.684+, is distinctly underbonded (bond-valence sum, BVS, of 1.619 valence units, vu), whereas the (Zr1,Ti1) site, with empirical occupancy ($Zr_{0.77}Ti_{0.12}Nb_{0.07}U_{0.025}Fe_{0.01}Hf_{0.005}$) and weighed formal charge of 4.052+, is slightly overbonded (BVS 4.161 vu). The BVS of O1 and O2 are much lower than 2 (1.596 and 1.757 vu, respectively), strongly indicating the partial substitution of F for O at these sites, which agrees with the chemical-analytical data (Table 2). Tentative refinements of the occupancy of the O1 and O2 sites gave values of 1.21(4) and 1.08(4) for holotype steiningerite, and 1.141(14) and 0.984(14) for the crystal studied by Kolitsch et al. (2003). The extent of F-for-O substitution at the O1 site thus is appreciable, although the exact F content cannot be determined reliably by such a refinement, considering the heavy elements present in the structure. The incorporation of considerable K at the Ba site is mainly counterbalanced by the incorporation of considerable F at the O1 site [also a ligand of the (Ba,K) atom, at the very long distance of 3.259(1) Å; Table 5], the charge-balancing substitution scheme likely is $Ba^{2+} + K^{+} \leftrightarrow O^{2-} + F^{-}$. The oxygen ligands O3, O4 and O5 are slightly overbonded.

https://doi.org/10.1180/mgm.2024.102 Published online by Cambridge University Press

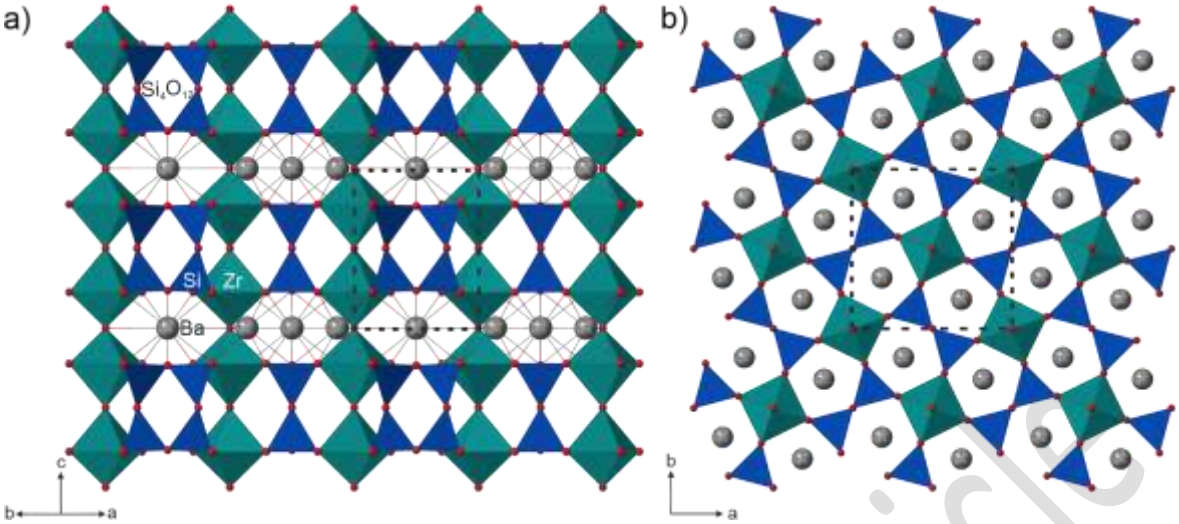

Fig. 6. a) Crystal structure of steiningerite, in a projection along [110], composed of $(Zr,Ti)O_6$ octahedra (marine-green), and Si_4O_{12} rings (dark blue). The $(Ba,K)O_{12}$ polyhedra have been omitted for clarity; instead, the (Ba,K) atoms are shown as grey spheres bonded to the red O atoms; b) The pentagonal channels occupied by (Ba,K) atoms formed by heterocyclic rings comprised of two $(Zr,Ti)O_6$ octahedra and three SiO_4 tetrahedra (projection along [001]). The unit-cell is outlined by a dotted line.

Table 3. Atom coordinates, equivalent displacement parameters (U_{eq}, Å^2) and site occupancies of steiningerite.

Site	Atom	*x*	*y*	*z*	U_{eq}	Occupancy
Ba1	Ba	0.68202(6)	0.18202(6)	0	0.0247(2)	0.645(8)
K1	K					0.355(8)
Zr1	Zr	0	0	0.25683(11)	0.0180	0.944(16)
Ti1	Ti					0.056(16)
Si1	Si	0.37699(13)	0.12301(13)	0.6981(2)	0.0174(4)	1
O1	O	0	0	0	0.0231(18)	1
O2	O	0	0	0.5	0.031(2)	1
O3	O	0.5	0	0.2341(8)	0.0283(15)	1
O4	O	0.2189(4)	0.0747(4)	0.2241(4)	0.0295(10)	1
O5	O	0.3770(6)	0.1230(6)	0.5	0.0287(15)	1

Note: For discussion of F-for-O substitution at the underbonded O1 and O2 sites, see text.

https://doi.org/10.1180/mgm.2024.102 Published online by Cambridge University Press

Table 4. Anisotropic displacement parameters (Å^2) of steiningerite.

Site	Atom	U^{11}	U^{22}	U^{33}	U^{12}	U^{13}	U^{23}
Ba1 K1	Ba K	0.271(3)	0.271(3)	0.0201(4)	-0.0077(3)	0	0
Zr1 Ti1	Zr Ti	0.0157(3)	0.0157(3)	0.0225(5)	0	0	0
Si1	Si	0.0185(6)	0.0185(6)	0.0152(8)	0.0007(6)	0.0002(4)	-0.0002(4)
O1	O	0.032(3)	0.032(3)	0.005(3)	0	0	0
O2	O	0.038(3)	0.038(3)	0.017(4)	0	0	0
O3	O	0.034(2)	0.032(2)	0.016(3)	0.012(3)	0	0
O4	O	0.0231(16)	0.0359(19)	0.0294(17)	-0.0039(15)	-0.0045(13)	0.0039(15)
O5	O	0.034(2)	0.034(2)	0.018(3)	0.005(3)	0	0

Table 5. Selected interatomic distances (Å) and cation site occupancies of the empirical formula (normalised to 1.00) used to calculate the weighted bond valences (in valence units, vu); (qX) – mean oxidation number of cations; (qA) – anion oxidation number; (BVS) – bond valence sum.

Site 1	Site 2	Distance
(Ba1,K1)	O3	2.965(4) × 2
$Ba_{0.65}K_{0.28}Na_{0.04}Sr_{0.02}Ca_{0.01}$	O4	2.836(4) × 4
	O4	3.040(4) × 4
	*O1	3.259(1) × 2
	Mean	2.996
	qX	1.684
	BVS	1.619
(Zr1,Ti1)	O1	2.067(1) × 1
$Zr_{0.77}Ti_{0.12}Nb_{0.07}U_{0.025}Fe_{0.01}Hf_{0.005}$	O2	1.957(1) × 1
	O4	2.074(3) × 4
	Mean	2.053
	qX	4.052
	BVS	4.201
Si1	O3	1.641(3) × 1
$Si_{0.99}Al_{0.01}$	O4	1.598(4) × 2
	O5	1.595(2) × 1
	Mean	1.608
	qX	3.992
	BVS	4.174
O1	Zr1/Ti1	2.067(1) × 2
	Ba1/K1	3.259(1) × 4
	qA	2

https://doi.org/10.1180/mgm.2024.102 Published online by Cambridge University Press

	BVS	1.596
O2	Zr1/Ti1	1.957(1) × 2
	qA	2
	BVS	1.757
O3	Ba1/K1	2.965(4) × 2
	Si1	1.641(3) × 2
	qA	2
	BVS	2.191
O4	Ba1/K1	3.040(4)
	Ba1/K1	2.836(4)
	Zr1/Ti1	2.074(3)
	Si1	1.598(4)
	qA	2
	BVS	2.026
O5	Si1	1.595(2) × 2
	qA	2
	BVS	2.156

*(Ba1,K1)–O1 = 3.259(1) Å, corresponding to 0.07 vu

Because attempts to collect X-ray powder diffraction data were unsuccessful, the powder XRD pattern was calculated with the program VESTA using the results of the single-crystal structure refinement (Table 6).

Table 6. Calculated X-ray powder diffraction data for steiningerite (λ = 0.71073 Å). Lines with relative intensities below 3% are omitted.

I[%]	*d*[Å]	*h*	*k*	*l*	*I*[%]	*d*[Å]	*h*	*k*	*l*
51.15	8.0510	0	0	1	6.30	1.8161	3	2	3
17.16	6.2890	1	1	0	12.64	1.7830	4	2	2
10.53	4.4470	2	0	0	8.08	1.7443	5	1	0
13.86	4.0255	0	0	2	3.80	1.7047	5	1	1
36.93	3.8927	2	0	1	10.51	1.6952	2	2	4
100.0	3.5661	2	1	1	6.80	1.6813	4	1	3
19.10	3.3904	1	1	2	4.63	1.6520	3	3	3
32.14	3.1445	2	2	0	17.94	1.6368	3	1	4
71.10	2.9844	2	0	2	3.75	1.6179	5	2	1
4.11	2.9290	2	2	1	16.93	1.6005	5	1	2
77.41	2.8293	2	1	2	6.89	1.5722	4	4	0
66.14	2.8125	3	1	0	8.45	1.5253	5	3	0
8.00	2.6837	0	0	3	6.84	1.4986	5	3	1
3.98	2.4667	3	2	0	9.67	1.4925	2	1	5
5.10	2.2977	2	0	3	4.43	1.4823	6	0	0
9.57	2.2246	2	1	3	9.83	1.4716	4	1	4
24.12	2.1571	4	1	0	4.88	1.4645	4	4	2

https://doi.org/10.1180/mgm.2024.102 Published online by Cambridge University Press

22.37	2.0836	4	1	4	3.71	1.4622	6	1	0
5.09	2.0413	2	2	3	10.91	1.4147	4	2	4
7.59	2.0287	3	3	1	11.36	1.3276	6	2	2
24.70	2.0127	0	0	4	4.98	1.2903	4	1	5
23.11	1.9888	4	2	0	3.96	1.2846	2	0	6
6.10	1.9463	4	0	2	8.39	1.2157	5	3	4
12.25	1.9416	3	1	3	4.01	1.1936	6	0	4
3.30	1.9170	1	1	4	3.20	1.1301	3	3	6
5.39	1.9013	4	1	2	3.07	1.0786	8	2	0
14.07	1.8593	3	3	2	3.79	1.0716	8	0	2

Discussion

The ideal end-member formula of steiningerite may be presented as $BaZrSi_2O_7$, similar to the established formulae of the chemically related compounds $SrZrSi_2O_7$, $CaZrSi_2O_7$ (gittinsite), $BaTiSi_2O_7$ and $SrTiSi_2O_7$, all of which have surprisingly different crystal structures. However, the shortened form may erroneously suggest that steiningerite is a sorosilicate with $(Si_2O_7)^{6-}$ units. Therefore, we proposed the doubled formula, which was approved by CNMNC IMA to emphasise the structural relationship with cyclosilicates.

The bond-valence analysis shows that the BVS at O1 and O2 is 1.60 and 1.76 vu, respectively (Table 5). These values are closer to 2 than 1, suggesting that O^{2-} prevails over F^- at both O1 and O2 sites, and that F is disordered over O1 and O2. To avoid the proliferation of possible new (O,F)-species, we propose to merge the chemical composition at O1 and O2. This merging leads to the definition of the boundary between the approved end-member $Ba_2Zr_2(Si_4O_{12})^{O(1,2)}(O_2)$ and the theoretical end-member $K_2Zr_2(Si_4O_{12})^{O(1,2)}(F_2)$ as $(BaK)Zr_2(Si_4O_{12})^{O(1,2)}(OF)$, with O > F for O-species and F > O for F-species at the combined (O1 + O2) sites.

Steiningerite is isotypic with the synthetic compound $KTaSi_2O_7$ (Lee et al. 1996) and closely related to the ferroelectric compound $KNbSi_2O_7$ (non-centrosymmetric space group *P*4*bm*; Crosnier et al. 1991, 1992; Foster et al. 1999), which is a synthetic analogue of rippite,

https://doi.org/10.1180/mgm.2024.102 Published online by Cambridge University Press

$K_2(Nb,Ti)_2(Si_4O_{12})(O,F)_2$ (Sharygin et al. 2020). Furthermore, a close structural relationship also exists with $K_4Sc_2(OH)_2(Si_4O_{12})$ (pseudo-tetragonal, space group *Pbam*; Pyatenko et al. 1979), whose formula can be rewritten as $K_2Sc(Si_2O_6)(OH)$. The centrosymmetric structures of $KTaSi_2O_7$ and steiningerite show a small but intriguing difference with the respect to the behaviour of the central atom in the octahedron. The Zr atom in steiningerite, like the Ta atom in $KTaSi_2O_7$, are both located on the fourfold axis and in a mirror plane. However, whereas the Zr atom is placed at the centre of the octahedron in steiningerite, the Ta atom in $KTaSi_2O_7$ occupies a split position (Lee et al. 1996). Thus, the Ta atoms are displaced from the mirror plane for about 0.19 Å within the octahedra, resulting in different Ta–O bond lengths (Lee et al. 1996). Despite having a lower symmetry, the structure of the non-centosymmetric rippite is similar to both above-mentioned structures (Sharygin et al. 2020; Fig. 7a-c). The absence of a mirror plane in rippite leads to the splitting of Nb, Si and O sites into symmetrically non-equivalent sites. However, the presence of differently large and charged cations at the centre of the octahedra has a slight influence on the symmetry of the Si_4O_{12} rings within the structures. Comparing the four-membered rings in the three structures (Fig. 7), we can observe very similar Si-O-Si angles in $KTaSi_2O_7$ (Si1-O5-Si1 = 175.5˚, Si1-O3-Si1 = 136.8˚), rippite (Si2-O5-Si1 = 176.7; Si2-O7-Si2 = 139.9˚), and steiningerite (Si1-O5-Si1 = 180˚; Si1-O3-Si1 = 141.1˚), respectively, reflecting the stiffening of the rings. Comparing the bond lengths of SiO_4 tetrahedra, one can see that in $KTaSi_2O_7$ and steiningerite the Si1–O3 bond is the longest [1.639(4) Å and 1.641(3) Å, respectively) and the Si1–O5 bond the shortest (1.588(3) Å and 1.5949(17) Å]. In rippite, there are two differently disordered tetrahedra: $Si1O_4$ tetrahedra has the longest bond Si1–O6 = 1.644(3) Å, and the shortest bond Si1–O5 = 1.540(7) Å, whereas $Si2O_4$ has two longer bonds to oxygen atoms shared with $Si1O_4$, Si2–O5 = 1.640(7) Å, Si2–O7 = 1.632(3) Å, and two shorter bonds to octahedra, Si2–O2 = 1.590(5) Å.

https://doi.org/10.1180/mgm.2024.102 Published online by Cambridge University Press

The isomorphic substitution scheme $(Ta,Nb)^{5+} + K^{+} \leftrightarrow Zr^{4+} + Ba^{2+}$ among the synthetic and natural mentioned phases suggest that steiningerite and rippite may be members of a new mineral group.

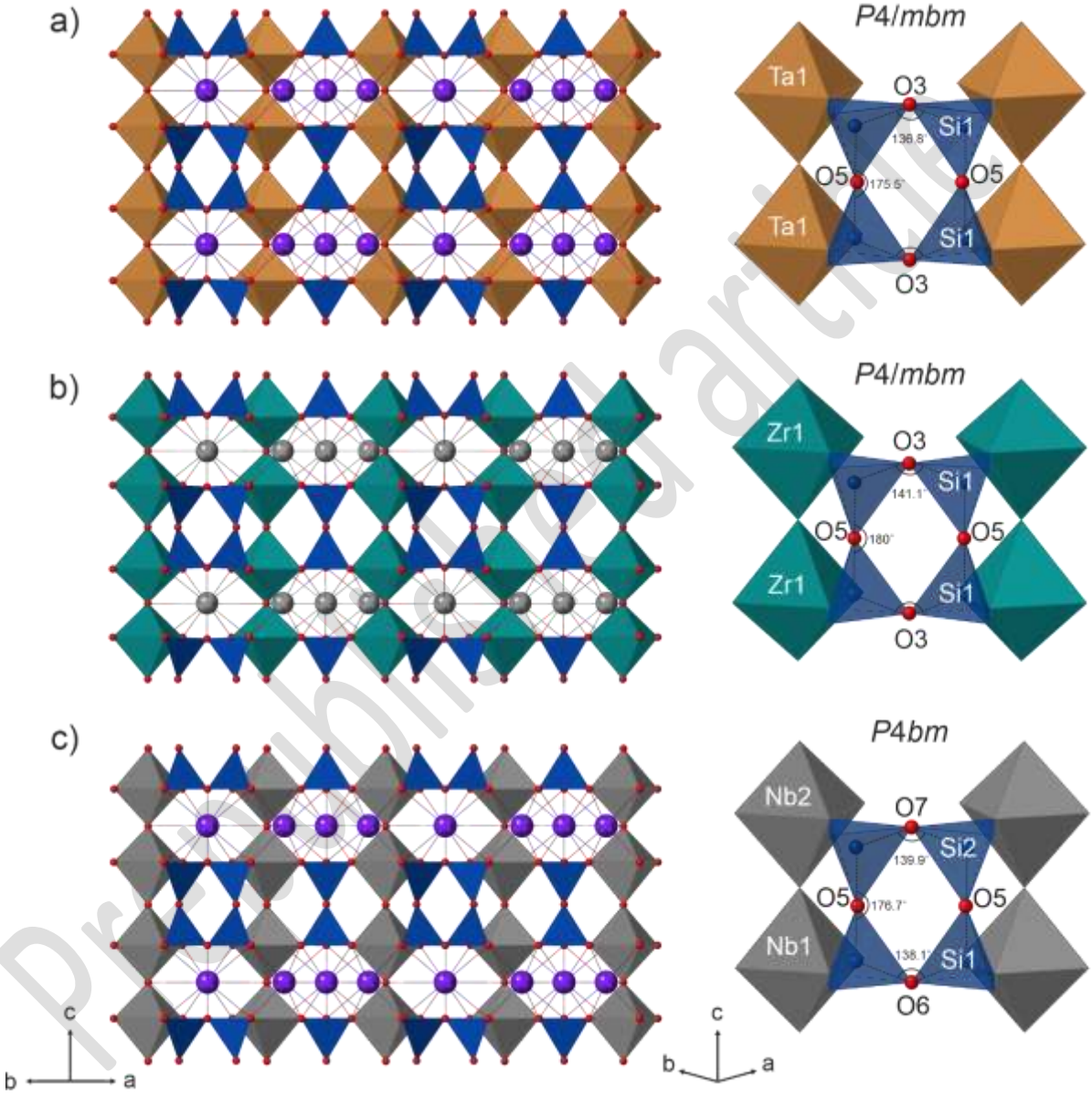

Fig. 7. Crystal structure of $KTaSi_2O_7$ (a), steiningerite (b) and rippite (c) and their Ta,Zr,Nb-Si_4O_{12} linkage. Brown – TaO_6 octahedra, marine-green – ZrO_6 octahedra, grey – NbO_6 octahedra and blue – Si_4O_{12} rings. Ba and K atoms are shown as grey and purple spheres, respectively.

https://doi.org/10.1180/mgm.2024.102 Published online by Cambridge University Press

With respect to other cyclosilicates containing Si_4O_{12} rings, steiningerite shows, as already briefly pointed out by Kolitsch et al. (2003), a close structural relation also with the labuntsovite-supergroup minerals, namely with members of the nenadkevichite group (Chukanov et al. 2002). In the crystal structure of the nenadkevichite-group members (e.g. nenadkevichite, $(Na,\square)_8Nb_4(Si_4O_{12})_2(O,OH)_4 \cdot 8H_2O$), chains of vertex-linked NbO_6 or TiO_6 octahedra extending along the pseudo-tetragonal *a* axis exist, as well as Si_4O_{12} rings. However, these rings are oriented parallel to [100] direction, which means they are rotated by 90˚ with respect to the chain orientation in steiningerite. It is worth mentioning that in comparison to the nenadkevichite-group members, steiningerite is nominally free of H_2O and OH groups, which was confirmed by the spectroscopic investigations.

We are not aware of any report of a synthetic analogue of steiningerite although it can be assumed that a high-temperature solid-state or flux-growth synthesis of steiningerite should be easily possible. The occurrence of steiningerite within fissures and cavities of a melilite nephelinite, along with its high-temperature mineral association, suggest that it has formed either at high-temperature hydrothermal or pneumatolytic conditions. This hypothesis is consistent with previous suggestions in connection with new mineral discoveries at the Löhley quarry (Chukanov et al. 2011, 2012). In the original description of lileyite, $Ba_2Ti_2Na_2Fe^{2+}Mg(Si_2O_7)_2O_2F_2$, the authors showed that the new mineral and all associated primary minerals contain neither hydroxyl nor H_2O molecules, in common with the assemblage containing steiningerite. This indicates high-temperature conditions and suggests a pneumatolytic rather than a low-temperature hydrothermal origin (Chukanov et al. 2012).

https://doi.org/10.1180/mgm.2024.102 Published online by Cambridge University Press

Supplementary materials

This section includes cif and check-cif files of holotype steiningerite; Steiningerite approval letter from IMA CNMNC.

Acknowledgements

The authors thank Mr Volker Heck for optical photomicrographs of steiningerite and associated minerals and Mr Frank de Wit for the macro photo of the Löhley quarry. Grzegorz Zieliński from the Micro-Area Analysis Laboratory, Polish Geological Institute, National Research Institute, is thanked for help with the electron microprobe analyses, and Mateusz Dulski and Dorota Środek from the University of Silesia for help with FTIR measurements. Mr Franz-Josef Emmerich, Cologne, Germany, is thanked for providing material for study. Hans-Jürgen Bernhardt is thanked for measuring EPMA data for the material provided by Mr Emmerich and Olaf Medenbach is thanked for optical measurements of the same material; Christian Lengauer, University of Vienna, measured a Gandolfi powder diffraction pattern of this material, and Werner Krause measured its density.

Competing interests

The authors declare none.

References

Chukanov N.V., Pekov I.V., Rastsvetaeva R.K., Aksenov S.M., Zadov A.E., Van K.V., Blass G., Schüller W., Ternes B. (2012) Lileyite, $Ba_2(Na,Fe,Ca)_3MgTi_2(Si_2O_7)_2O_2F_2$, a new lamprophyllite-group mineral from the Eifel volcanic area, Germany. *European Journal of Mineralogy*, **24** (1), 181–188.

Chukanov N.V., Rastsvetaeva R.K., Britvin S.N., Virus A.A., Belakovskiy D.I., Pekov I.V., Aksenov S.M., Ternes B. (2011) Schüllerite,

https://doi.org/10.1180/mgm.2024.102 Published online by Cambridge University Press

$Ba_2Na(Mn,Ca)(Fe^{3+},Mg,Fe^{2+})_2Ti_2(Si_2O_7)_2(O,F)_4$, a new mineral species from the Eifel Volcanic District, Germany. *Geology of Ore Deposits*, **53** (8), 767–774.

Chukanov N.V., Pekov I.V., Khomyakov A.P. (2002) Recommended nomenclature for labuntsovite-group minerals. *European Journal of Mineralogy*, **14** (1), 165–173.

Chukanov N.V. (2014) Infrared spectra of mineral species: Extended library. Springer-Verlag GmbH , Dordrecht, Netherlands, 1716 pp.

Crosnier M.P. , Guyomard D., Verbaere A., Piffard Y., Tournoux M. (1992) The potassium niobyl cyclotetrasilicate $K_2(NbO)_2Si_4O_{12}$. *Journal of Solid State Chemistry*, **98** (1), 128–132.

Crosnier M.P., Guyomard D., Verbaere A., Piffard Y., Tournoux M. (1991) $K_2(NbO)_2Si_4O_{12}$: A new material for non-linear optics. *Ferroelectrics*, **124**, 61–66.

Foster M.C., Arbogast D.J., Photinos P., Nielson R.M., Abrahams S.C. (1999) $K_2(NbO)_2Si_4O_{12}$: a new ferroelectric. *Journal of Applied Crystallography*, **32**, 421–425.

Hentschel G. (1987) Die Mineralien der Eifelvulkane. 2nd ed., Weise Verlag, München, Germany.

Ilinca G. (2022) Charge distribution and bond valence sum snalysis of sulfosalts - the ECoN21 computer program. *Minerals*, **12**, 924.

Kolitsch U., Lengauer C.L,. Krause W., Bernhardt H.-J., Medenbach O., Blaß G. (2003) $BaZrSi_2O_7$, a new mineral from the Eifel volcanic area, Germany. *Mitteilungen der Österreichischen Mineralogischen Gesellschaft*, **148**, 199–200.

Lee J.-G., Höhn P., Greenblatt M. (1996) A potassium tantalum (V) tetrasilicate $KTaSi_2O_7$. *Journal of Solid State Chemistry*, **123**, 123–128.

Lengauer C.L., Tillmanns E., Hentschel G. (2001) Batiferrite, $Ba[Ti_2Fe_{10}]O_{19}$, a new ferrimagnetic magnetoplumbite-type mineral from the Quaternary volcanic rocks of the western Eifel area, Germany. *Mineralogy and Petrology*, **71** (1), 1–19.

Mandarino J.A. (1989) The Gladstone-Dale compatibility of some new mineral proposals considered by the Commission on New Minerals and Mineral Names, I. M. A. (1983–1987). *European Journal of Mineralogy*, **1**, 123–125.

Mertes H. (1983) Aufbau und Genese des Westeifeler Vulkanfeldes. Bochumer Geologische und Geotechnische Arbeiten 9, 415 pp.

Palatinus L., Chapuis G. (2007) SUPERFLIP – a computer program for the solution of crystal structures by charge flipping in arbitrary dimensions. *Journal of Applied Crystallography*, **40**, 786-790.

Petříček V., Palatinus L., Plášil J., Dušek M. (2023) Jana2020 – a new version of the crystallographic computing system Jana. *Zeitschrift für Kristallographie - Crystalline Materials*, **238**, 271–282.

https://doi.org/10.1180/mgm.2024.102 Published online by Cambridge University Press

Pyatenko Yu.A., Zhanova T.A., Voronkov A.A. (1979) Crystal structure of $K_4Sc_2(OH)_2[Si_4O_{12}]$. *Doklady Akademii Nauk SSSR*, **248**, 868–871. (In Russian.)

Sharygin V.V., Doroshkevich A.G., Seryotkin Y.V., Karmanov N.S., Belogub E.V., Moroz T.N., Nigmatulina E.N., Yelisseyev A.P., Vedenyapin V.N., Kupriyanov I.N. (2020) Rippite, $K_2(Nb,Ti)_2(Si_4O_{12})O(O,F)$, a new K-Nb-cyclosilicate from Chuktukon Carbonatite Massif, Chadobets Upland, Krasnoyarsk Territory, Russia. *Minerals*, **10**, 1102.

Uvarova Y.A., Sokolova E., Hawthorne F.C., Liferovich R.P., Mitchell R.H., Pekov I.V., Zadov A.E. (2010) Noonkanbahite, $BaKNaTi_2(Si_4O_{12})O_2$, a new mineral species: description and crystal structure. *Mineralogical Magazine*, **74**, 441–450.

https://doi.org/10.1180/mgm.2024.102 Published online by Cambridge University Press